Intersubband carrier relaxation in highly excited GaAs/$Ga_{1-x}Al_xAs$ multiple quantum wells

J. A. Levenson, G. Dolique, J. L. Oudar, and I. Abram
Laboratoire de Bagneux, Centre National d'Etudes des Telecommunications, 196 avenue Henri Ravera, 92220 Bagneux, France
(Received 25 September 1989)

We investigate the dynamics of the intersubband relaxation of electrons by injecting photoexcited carriers in the first three subbands of GaAs/$Ga_{1-x}Al_xAs$ multiple quantum wells. The intersubband relaxation rate is measured as a function of the subband separation energy by using samples with different well widths. While the electron–LO-phonon interaction appears to be the dominant energy-dissipation mechanism, the relaxation rate displays a very slow variation and not an abrupt threshold at the LO-phonon energy, when the energy separation is varied. A simple model taking into account the finite electronic temperature and the occupation of final states can explain our results.

I. INTRODUCTION

Recent experimental studies[1–3] on the dynamics of photoexcited carriers in bulk semiconductors and multiple quantum wells (MQW's) have shown that the **k**-vector relaxation of the photoinduced population and the establishment of a quasiequilibrium thermal distribution of electron-hole pairs occur in a very short time scale, essentially in a few hundreds of femtoseconds. The population of quasiequilibrium electrons and holes is observed subsequently to cool down to the lattice temperature,[4] on a time scale that may extend to several tens of picoseconds. These time scales have the same order of magnitude in three-dimensional bulk semiconductors and in two-dimensional MQW's, and can be conceived in the same theoretical framework,[5,6] once allowance is made for the different dimensionalities. These two relaxation regimes are understood to result from the interplay of two elementary interaction mechanisms: carrier-carrier scattering and carrier-phonon interactions. Thus, the establishment of a thermal carrier distribution is attributed essentially to carrier-carrier collisions which conserve the average energy per carrier, while the cooling process involves a net energy loss from the electronic subsystem, and is understood to occur through the emission of polar-optical or acoustical phonons as the carriers undergo transitions to lower-energy states. Throughout the cooling process, carrier-carrier scattering maintains at all times a thermal distribution. In polar semiconductors like GaAs and GaAs/$Ga_{1-x}Al_xAs$ MQW's and at carrier temperatures higher than 50 K the interaction with longitudinal optical (LO) phonons is expected to be the principal energy-loss mechanism for the carriers while the acoustical-phonon interaction is expected to be weak.[4]

In MQW's, an additional feature has to be taken into account when considering carrier relaxation. The confinement of the carriers in the ultrathin semiconductor layers produces a quantization of the carrier momentum perpendicular to the layers (z axis) and gives rise to a splitting of the valence and conduction bands into a series of subbands. Thus, in addition to thermalization and cooling of the carriers within each subband, the carriers may relax between the different subbands. Conceptually, the intersubband relaxation process is differentiated from the intrasubband thermalization and cooling simply by the fact that momentum is quantized and discrete in the former case, while it is continuous in the latter. In fact, in the limit of wide quantum wells the quantized z momentum becomes quasicontinuous, and thus the (two-dimensional) intrasubband and the intersubband processes fuse into the same (three-dimensional) momentum and energy relaxation process.

Intersubband relaxation occurs by different mechanisms: LO-phonon emission, acoustic-phonon emission, and carrier-carrier interactions such as the Auger effect. Interaction with LO phonons is expected to be the principal intersubband relaxation mechanism, since electron–acoustic-phonon[7] and Auger[8] interactions are expected to take place in times of the order of a few hundred picoseconds for carrier densities less than 10^{12} cm^{-2}.

In a very recent experiment, Tatham *et al.*[9] have demonstrated an intersubband relaxation time shorter than 1 ps for a MQW (146-Å-wide well) by use of time-resolved Raman scattering measurements under very low photoexcited carrier density. This result is in good agreement with theoretical predictions.[10,11] Several experiments have been performed in order to determine the intersubband relaxation times in MQW's under high carrier excitation density. In one type of experiment,[12,13] the first electronic subband of a MQW is populated by modulation doping and the bleaching of the 1 to 2 intersubband transition is measured by a pump-and-probe technique, directly in the infrared. The measured characteristic relaxation times are of the order of 10 ps, at room temperature, for intersubband splittings of about 150 meV (well widths of the order of 50 Å), and are attributed to LO-phonon emission. In a second type of experiment,[14] an electron-hole plasma is optically injected in the first and second subbands of a MQW, and the time evolution of the electron population is monitored through electronic Raman scattering. The measured relaxation times are of the order of 10 ps for an intersubband energy

difference of the order of 64 meV (116-Å-wide wells), and 500 ps for an intersubband spacing of 27 meV (215-Å-wide wells). This slowing down of the electronic intersubband relaxation was interpreted as evidence for the participation of the LO phonons in the energy-loss mechanism: the energy relaxation practically stops when the electrons of the second subband cannot undergo a transition by emitting an LO phonon of 36.7 meV.

In this paper we present a different experimental approach to the measurement of intersubband relaxation. As in the experiments of Oberli *et al.*,[14] a short and intense light pulse incident on a MQW injects a large population of electrons and holes in their respective first and second subbands. However, in our experiments the time evolution of the subband populations generated by that pulse is measured through the bleaching induced on the transmission of a second (probe) pulse. We find that the intersubband relaxation is indeed slower for transitions between states separated by less than the energy of one LO phonon. However, the bleaching recovery time is always shorter than 40 ps, even in the case in which the intersubband splitting is smaller than the LO-phonon energy. As explained in this paper, this result suggests that (1) the carriers in all subbands have a common temperature, even if in the higher subbands they are injected with no kinetic energy, and (2) the intersubband relaxation essentially proceeds through the high-energy tail of the electron distribution, i.e., the part of the distribution which has enough kinetic energy to emit LO phonons.

The paper is organized as follows. Section II presents the experimental setup. The dynamics of the bleaching in the two first subbands is analyzed in Sec. III. Section IV deals more particularly with the carrier intersubband relaxation time as a function of the well width. In Sec. V we present some simple calculations of the intersubband scattering rate within the MCA approximation. Finally, Sec. VI contains the conclusions of this study.

II. EXPERIMENTAL

The light source consists of two simultaneously pumped traveling-wave optical parametric generators (OPG's), each composed of two $LiIO_3$ crystals in a double-pass configuration (total amplification length of 10 cm). The OPG's are pumped at 532 nm (2340 meV) by the second harmonic of a pulsed mode-locked Nd^{3+}-doped yttrium aluminum garnet (YAG) laser, which delivers 50-ps-long pulses at 20-Hz repetition rate. Each OPG can be scanned in wavelength independently of the other, between 0.7 and 2 μm (1700 and 600 meV) by angle tuning the $LiIO_3$ crystals. Each OPG produces 12-ps-long pulses, having a spectral width of the order of 1 meV and a peak intensity that can attain 100 MW/cm^2 ($\sim$1 mJ/cm^2) upon focusing on the sample. The light source is described in more detail in Ref. 15. As the two OPG's are pumped by the same laser pulse, their output pulses are synchronized to better than 1 ps. The two pulses can be delayed with respect to each other by adjusting their relative path length before reaching the sample. Each path length can be adjusted to better than 30 μm, corresponding to a definition of better than 0.2 ps in the relative delay of the two pulses.

The output pulses of the two OPG's are used in a pump-and-probe configuration in which one pulse of fixed wavelength (pump) excites the sample in resonance with an excitonic transition while the other (probe) is scanned in wavelength or in time delay to measure the transmission spectrum of the photoexcited sample at different pump-probe delays or the bleaching recovery at different wavelengths. The probe beam is attenuated enough so as not to produce any nonlinear effect (i.e., at most 10^{10} cm^{-2} photoinduced carriers in a layer). The pump beam is focused into a spot diameter of about 250 μm while the probe is focused into a smaller spot (200 μm), centered on the "pump" spot. A tighter focus of the probe beam was chosen in order to minimize the effects of the transverse inhomogeneity of the Gaussian beam profiles. The data are recorded on a shot-to-shot basis, and an electronic discriminator rejects all shots for which the pump intensity (I_p) lies outside a given range, thus enabling data recording at constant I_p. A reference beam is split out of the probe beam by inserting a 4% beam splitter in its path. By taking the ratio of the reference and probe beam intensities each spectrum can thus be corrected for the pulse-to-pulse intensity fluctuations of the probe. All the optical signals are detected by means of Si photodiodes. As these photodiodes have a slow response time ($\sim$10 μs), the time resolution of our experiments (a few ps) is obtained by purely optical means. The data acquisition, as well as the wavelength and delay scans, are controlled by a computer.

The samples investigated here are molecular-beam-epitaxy (MBE) -grown GaAs/$Ga_{0.7}Al_{0.3}As$ multiple quantum wells, each sandwiched between two 1-μm-thick $Ga_{0.7}Al_{0.3}As$ layers. Sample *A* (*B*, *C*) consists of 60 periods (30 periods) of 120-Å (225 Å, 240 Å) -wide wells and 75-Å-wide barriers, as measured by x-ray diffraction. The GaAs layers are unintentionally doped with *p*-type residual doping of 5×10^9 cm^{-2}. A 2 mm^2 hole was chemically etched in the GaAs substrate to allow optical transmission experiments in the MQW. Al_2O_3 antireflection coatings were deposited to reduce Fabry-Perot effects. The sample temperature was reduced to 15 K by means of a closed-cycle He refrigerator.

Figure 1 reproduces the linear absorption spectra of both samples. The peaks labeled E_nH_m (E_nL_m) are the excitons built from a conduction electron E_n and a valence heavy-hole H_m (or light-hole L_m). The subscript n (or m) is the subband index, and refers to the nth (or mth) bound state of the corresponding quasiparticle in the quantum wells. All these transitions, except for the one labeled E_2L_1 (sample *A*), are allowed by the parity optical selection rules. The peak attributed to E_2L_1 probably occurs because of mixing between heavy- and light-hole states as suggested by Miller *et al.*[16] This hypothesis is confirmed in our experiments by the observation that the E_2L_1 transition is less stable with respect to optical excitation than E_2H_2 and its saturation follows the single-particle occupation of the L_1 subband rather than those of H_2 (see Secs. III and IV).

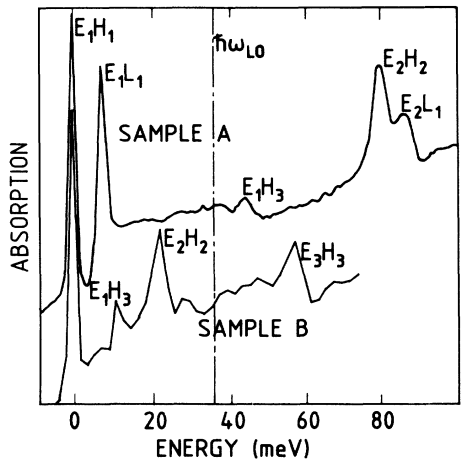

FIG. 1. Absorption spectra of two unexcited $GaAs/Ga_{0.7}Al_{0.3}As$ MQW samples. In sample A the well width is 120 Å while in sample B it is 225 Å.

III. DYNAMICS OF THE SPECTRAL MODIFICATIONS UNDER EXCITATION

The series of experiments performed on each sample follows a sequence of three steps. First we measure the linear spectrum of the sample (no pump). Then we tune the pump pulse to the E_1H_1 peak and thus introduce carriers in E_1H_1 while keeping E_2H_2 empty. This permits us to record the spectral modifications due to the presence of a dense plasma in E_1H_1 and gives a baseline for the experiments performed in the third step. Finally, the pump is tuned to E_2H_2, injecting carriers into this subband and on the high-energy part of the E_1H_1 subband. In this third step we observe the spectral modifications produced by the injection of carriers in E_2H_2 as a function of the pump wavelength and/or the delay time between the pump and the probe pulses. We display here (Figs. 2 and 3) the results obtained with sample A.

Figure 2 shows the excited spectra (dashed lines) in the vicinity of the E_1H_1 (E_1L_1) and the E_2H_2 excitons for selected probe delays when the pump pulse is in resonance with E_1H_1, with unexcited spectra (solid line) shown for reference. The excitation energy density is $I_p = 80\ \mu J/cm^2$ per pulse and corresponds to an estimated density of photoexcited carriers of $3.5\times10^{11}\ cm^{-2}$ per layer. The optical saturation of the E_1H_1 (E_1L_1) reaches a maximum at 10-ps probe delay, the probe pulse arriving just after the full pump-pulse energy is deposited in the sample. As shown in a previous paper,[17] the spectral modifications observed in the first and second subbands arise from different physical mechanisms. The strong optical saturation of E_1H_1 (E_1L_1) excitons reflects the single-particle occupation effects due to the direct phase-space filling, since the pump injects electrons and holes in these subbands [see Fig. 2(a)]. On the other hand, the exciton of the second subband E_2H_2 shows little optical saturation, but is broadened and shifted to lower energies by about 2.1 meV. Since this subband is unoccupied these changes are essentially a manifestation

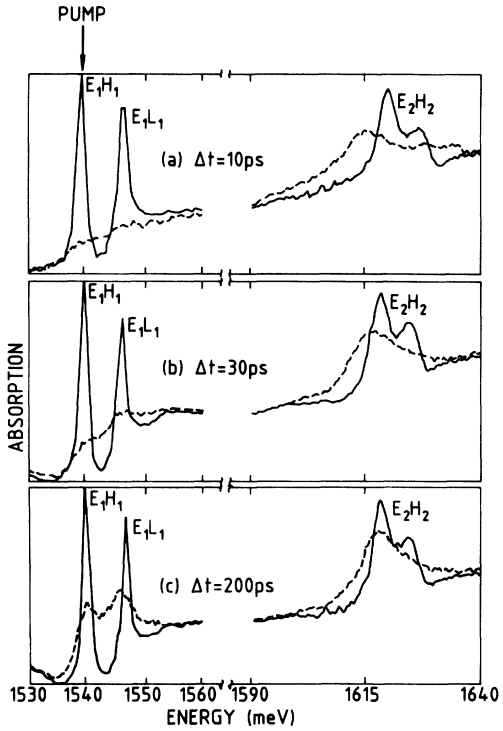

FIG. 2. Absorption spectra of unexcited (solid line) and excited (dashed line) sample A, around E_1H_1 (left-hand side) and around E_2H_2 (right-hand side) at three different probe delays: $\Delta t = 10$, 30, and 200 ps. The pump frequency (shown by arrow) is resonant with the E_1H_1 exciton.

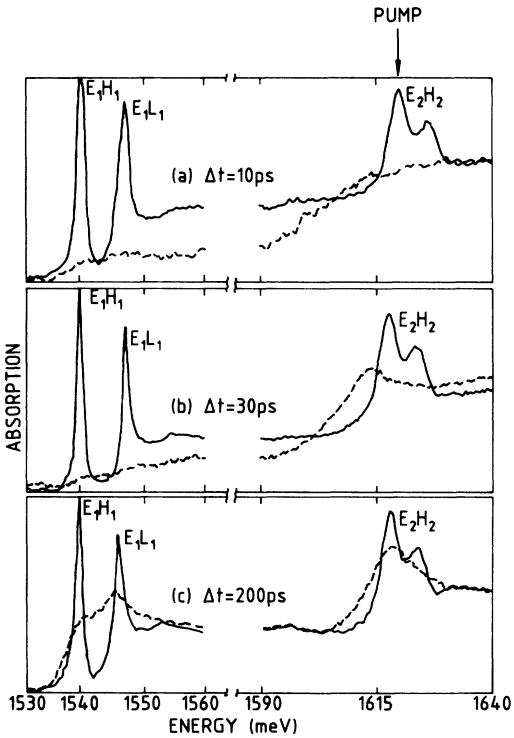

FIG. 3. Absorption spectra of unexcited (solid line) and excited (dashed line) sample A, around E_1H_1 (left-hand side) and around E_2H_2 (right-hand side) at three different probe delays: $\Delta t = 10$, 30, and 200 ps. The pump frequency (shown by arrow) is resonant with the E_2H_2 exciton.

of the many-body effects caused by the photoinduced population in E_1H_1 on the "test" quasiparticle injected by the probe pulse. After a few tens of ps, the high-energy part of the E_1H_1 (E_1L_1) band absorption recovers, but the lower-energy part displays a steplike feature without any excitonic line [see Fig. 2(b)]. At the same time the red shift of E_2H_2 decreases. Subsequently, the spectra remain constant during several hundred ps indicating that after 100 ps the carrier temperature reaches a quasiequilibrium; this regime is represented by the spectrum at 200-ps delay [see Fig. 2(c)]. In this quasiequilibrium regime the E_1H_1 (E_1L_1) excitonic lines reappear but are broadened, probably because of the exciton-exciton and free-carrier-exciton collisions.

These changes in the spectrum between 10 and 100 ps are consistent with a partial decay of the E_1H_1 population. Although radiative recombination usually occurs with a ns characteristic time at weak carrier densities,[18] this rapid population decay may be due to several mechanisms, such as the acceleration of the spontaneous radiative decay due to the high carrier concentration or the trapping of carriers.

Figure 3 shows the spectra obtained when the pump frequency is resonant with the E_2H_2 exciton while the pumping conditions and time delays are the same as those of Fig. 2. The photoinduced population is slightly larger, estimated at 7×10^{11} cm^{-2} per layer, since a larger proportion of the pump could be absorbed due to a weaker bleaching at the pump frequency. This difference in population is reflected in the extent of the saturation observed in the absorption spectrum. We note that when exciting the E_2H_2 exciton, some carriers are also injected in the high-energy states of the E_1H_1 and E_1L_1 bands which are at the same energy as the E_2H_2 exciton. These carriers relax very rapidly to the bottom of the first subband and bleach the corresponding excitons in a manner similar to the direct pumping of the E_1H_1 and E_1L_1 excitons.

In contrast to the results displayed in Fig. 2, the initial E_2H_2 optical saturation is strong and the excitonic line is completely bleached [see Fig. 3(a)]. This result can be attributed to the single-particle occupation effects which now occur for E_2H_2 since the pump is tuned to this resonance. Between 10 and 30 ps the optical saturation decreases and a red-shifted E_2H_2 excitonic line reappears [see Fig. 3(b)]. This observation clearly points to a transition between two regimes: as long as the E_2H_2 population is present, the E_2H_2 resonance is bleached, and the manifestations of the many-body effects are masked. This is the case before 30 ps. As the carriers scatter out of the E_2 and H_2 states, the single-particle occupation effects in the second subbands vanish and many-body effects now become visible, analogous to those observed when a dense population is injected in E_1H_1, as displayed in Fig. 3(b). After that, as the carriers relax to the bottom of the E_1H_1 subband, we observe a similar time evolution as in Fig. 2. In particular, a quasiequilibrium regime is reached in a time scale of the order of 100 ps.

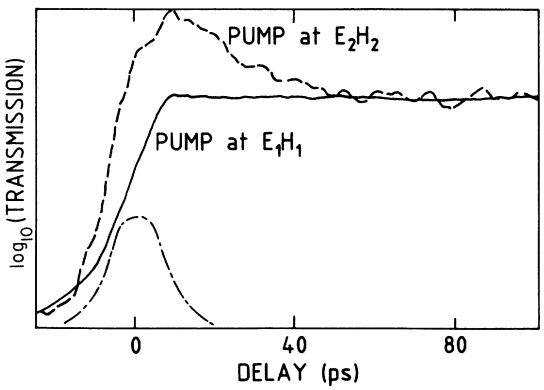

FIG. 4. Probe transmission at E_2H_2 as a function delay with respect to the pump. Solid line (dashed line) corresponds to the pump wavelength fixed at E_1H_1 (E_2H_2).

In samples B and C we found the same sequence of characteristic spectra but with a slightly different temporal evolution. In order to focus the discussion on the temporal aspect, let us describe the experimental curves for which the delay was scanned, rather than the wavelength.

In Fig. 4 we reproduce the time evolution of the probe transmission at E_2H_2 for sample B. The dashed (solid) curve corresponds to the pump wavelength fixed at E_2H_2 (E_1H_1). The cross-correlation between the pump and the probe pulses is also shown (dot-dashed curve). The maximum of the cross correlation indicates the zero-delay point (the pulses overlap completely). The maximum of transmission occurs when the probe pulse reaches the sample just after the end of the pump pulse (delay 10 ps). Following this maximum, when pumping at E_2H_2 (dashed curve) the time dependence of the transmission signal clearly shows two decay components: (1) a fast decrease of the transmission between 10 and 30 ps, and (2) a much slower behavior after 30 ps. The first feature is due to the E_2H_2 population relaxation already discussed. The possibility that this fast decay may be attributed to the depopulation through stimulated emission can be excluded, since such a mechanism must present a threshold as a function of the carrier density which was not observed in our experiments. At longer times the spectral changes of E_2H_2 are only produced by the effect of the dense E_1H_1 and E_1L_1 populations; thus the observed decay corresponds probably to the slow decay of E_1H_1 through mechanisms such as radiative recombination. This analysis is supported by the fact that both curves (pump at E_2H_2 and at E_1H_1) reach the same plateau as the E_2H_2 population relaxes down the E_1, H_1, and L_1 states.

Thus the comparison between the bleaching dynamics under E_2H_2 and E_1H_1 pumping allows to isolate the effect of the $2\rightarrow1$ intersubband relaxation, which is discussed in more detail in the next section.

IV. THE INTERSUBBAND RELAXATION

As discussed in Sec. I, the electron–LO-phonon interaction is expected to be the preferential channel by which carriers scatter from one subband to the other, and

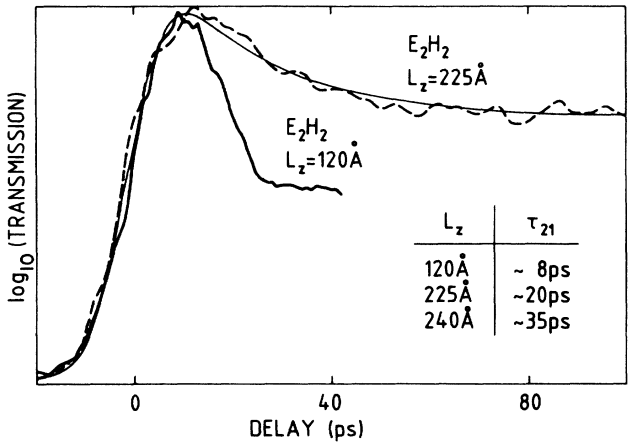

FIG. 5. Probe transmission at E_2H_2 as a function of the delay with respect to the pump. The pump is also fixed at E_2H_2. Solid line (dashed line) represents sample A (sample B). The thin line also shows the calculated curves in the two-level model.

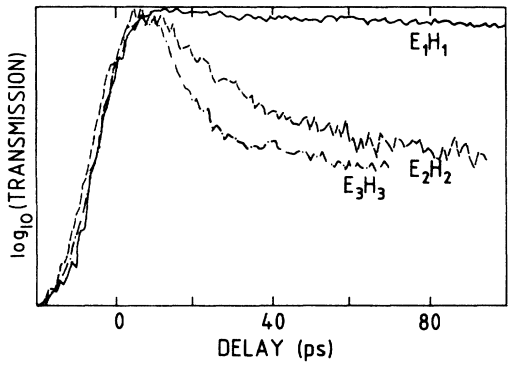

FIG. 6. Probe transmission as a function of the delay with respect to the pump (sample C). The pump and the probe are fixed at the same wavelength: E_1H_1 (solid line), E_2H_2 (dashed line), and E_3H_3 (dot-dashed line).

this could produce a threshold in the decay rate at the energy of the LO phonon.[14] Having in mind the possibility of observing such a threshold, we present a detailed comparison of results obtained with samples A and B. These samples were especially chosen in view of the energy separation of their first two electronic states: in sample A, the E_2H_2 energy corresponds (for electrons) to an excess energy of 65 meV, i.e., about twice the LO-phonon energy ($\hbar\omega_{LO}=36.7$ meV), while in sample B, the E_2H_2 energy corresponds to an excess energy of 20 meV, less than $\hbar\omega_{LO}$. Since the hole energies in our experiments are always less than $\hbar\omega_{LO}$, we will limit our discussion to electronic states. In addition, hole relaxation is expected to be faster by more than 1 order of magnitude than electron relaxation (that is, in a subpicosecond time scale).[19] Let us now present two series of experiments.

In Fig. 5 is reproduced the time evolution of the transmission of the probe at E_2H_2 for samples A (solid line) and B (dashed lines) when the pump is also fixed in resonance with the E_2H_2 exciton.

To evaluate the relaxation times, we may describe the temporal evolution of the E_2 population within the two-level model, which is a good approximation in the incoherent excitation regime.[20,21] When neglecting the pump depletion during propagation, the E_2 population n_2 follows the equation

$$\frac{\delta n_2(t)}{\delta t}=\alpha_0 I_p(t)\left[1-\frac{n_2(t)}{n_0}\right]-\frac{n_2(t)}{\tau_{21}}\ , \tag{1}$$

where n_0 is the number of possible states, α_0 is the linear absorption coefficient, $I_p(t)$ the temporal profile of the pump pulse intensity, and τ_{21} the intersubband relaxation time. The experimental decay is then given by the convolution of the temporal profile of the test beam I_t and the population evolution

$$R(t)=I_t(t)\otimes n_2(t,A)+R_1(t)\ , \tag{2}$$

where $R_1(t)$ is the experimental spectrum obtained when pumping at E_1H_1 and probing at E_2H_2 and takes into account the effect of the n_1 population on the n_2 spectrum (the plateau at times longer than 30 ps). Equations (1) and (2) were integrated numerically, and the parameters τ_{21} and A were adjusted so as to obtain the best fit with experimental curves.

The results for samples A and B are represented in thin lines in Fig. 5. The decay times τ_{21} could be evaluated as being on the order of 8±2 ps for sample A and 20±2 ps for sample B. The inset in Fig. 5 summarizes the relaxation time τ_{21} we found for samples A, B, and C.

Finally, Fig. 6 reproduces the time evolution of the transmission in sample C, at three pump and probe energies: E_1H_1 (solid line), E_2H_2 (dashed lines), and E_3H_3 (dot-dashed lines), the last two having an excess energy of 20 and 60 meV with respect to E_1H_1. The evolution of the slope of these curves shows a faster relaxation of the carriers with greater energies. This is similar to the behavior of bulk GaAs.[22] However, there is not a very large difference between curves E_2H_2 and E_3H_3 as the LO-phonon energy is crossed. In fact, the E_2H_2 relaxation is about 35±2 ps while the relaxation time of carriers injected in E_3H_3 is evaluated to be about 10±2 ps, comparable to the E_2H_2 relaxation in sample A for which the excess energy is 80 meV.

V. DISCUSSION

The small difference in the dynamics of bleaching recovery in our two samples raises some questions about the possibility of experimentally observing the threshold condition of the LO-phonon emission through a variation of well width. To discuss this point let us consider the electronic intersubband scattering rate (the inverse of the intersubband scattering time τ) in a simple way. In Fig. 7 the scattering rate of an electron from the second to the first subband (W_{21}) is plotted as a function of the well width (L_z) for different kinetic energies (ε_{kin}), which are measured in meV from the E_2 band edge. W_{21} is calculated in the momentum-conservation approximation (MCA), for infinite square wells and a single parabolic

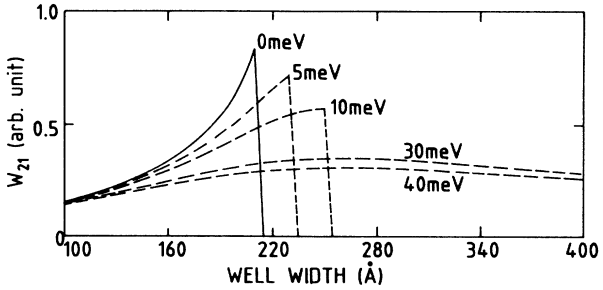

FIG. 7. Electron scattering rate (W_{21}) (in the MCA approximation) between the second and the first subbands as a function of the well width (L_z), for different kinetic energies measured from the E_2 band edge.

band, following Ridley.[23] The MCA approximation assumes that momentum conservation in MQW's is identical to that in the bulk. This crude approximation provides a simple analytical model giving the overall tendency of the scattering mechanism. More sophisticated models have been presented by several authors: Riddoch and Ridley,[24] Leburton,[25] Das Sarma and Mason,[26] Darling,[10] Goodnick and Lugli,[27] Ridley,[10] and Jain and Das Sarma.[11] Figure 7 for $\varepsilon_{\rm kin}=0$ shows that W_{21} increases as the well width increases but becomes suddenly zero when $E_2-E_1<\hbar\omega_{\rm LO}$. The maximum W_{21} (at $L_z=215$ Å) corresponds to the resonant case $E_2-E_1=\hbar\omega_{\rm LO}$. The increase of W_{21} between $E_2-E_1>\hbar\omega_{\rm LO}$ and $E_2-E_1=\hbar\omega_{\rm LO}$ underlines the fact that the wave vector $q_\parallel$ needed to allow in-plane momentum conservation becomes smaller as the well width increases ($W_{21}\propto 1/q_\parallel$). This tendency for the intersubband relaxation rate was experimentally pointed out by Seilmeier and co-workers[12] for well widths ranging between 47 and 66 Å ($\tau_{21}=14$ and 8 ps, respectively). As shown above for sample A ($L_z=120$ Å) we find $\tau_{21}=7$ ps, which is in good agreement with Seilmeier and co-workers.[12] When $\varepsilon_{\rm kin}>0$ the overall behavior is the same but the abrupt threshold is shifted and smoothed (see curves labeled 30 and 40 meV).

A more realistic calculation of the intersubband scattering rate when a warm electron population is involved requires averaging W_{21} over a thermal distribution of carriers. This situation translates more accurately our experimental conditions since the photoinjected carrier population becomes always thermalized at temperatures higher than the lattice temperature by carrier-carrier interaction (in a subpicosecond time scale). The measured intersubband relaxation time is thus an average of the relaxation time over a thermal distribution which contains carriers, some with and some without enough kinetic energy to emit LO phonons. The averaged intersubband scattering rate ($W_{21}^{\rm av}$) is given by

$$W_{21}^{\rm av}\propto\frac{1}{n_2}\frac{\delta n_2}{\delta t}\propto\frac{\int\delta E\,\rho_E f_2(E,T_2)[1-f_1(E-\hbar\omega_{\rm LO},T_1)]W_{21}}{\int\delta E\,\rho_E f_2(E,T_2)}, \tag{3}$$

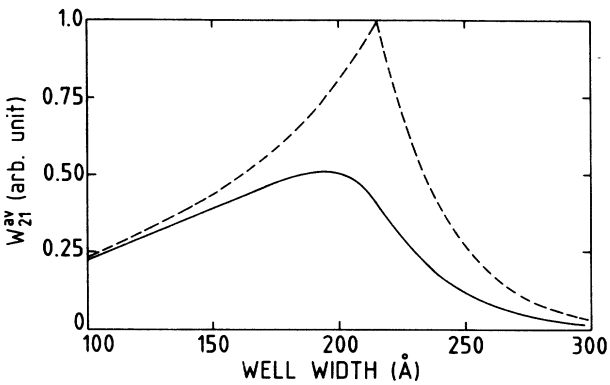

FIG. 8. Thermally averaged scattering rate ($W_{21}^{\rm av}$) between the second and the first subbands as a function of the well width (L_z). On the dashed line ($W_{21}^{\rm av}$) is represented when neglecting the final E_1 population.

where n_2 and $f_2(E,T_2)$ are the E_2 population and statistical distribution, $f_1(E,T_1)$ is the E_1 statistical distribution, and ρ_E the two-dimensional density of states.

In Fig. 8 (solid line) we reproduce $W_{21}^{\rm av}$ as a function of the well width, assuming a Maxwell-Boltzmann distribution. The carrier distribution has been calculated for each well width by considering a common temperature ($T_2=T_1$) for both subbands; that is, we consider a heating of $n=2$ electrons by the warm $n=1$ electrons also injected by the pump. This temperature is taken to be proportional to the excess kinetic energy in the first subband. Figure 8 clearly shows that $W_{21}^{\rm av}$ remains of the same order of magnitude at all well widths. The main feature is that $W_{21}^{\rm av}$ increases as the well width increases and becomes maximal around $L_z=215$ Å ($E_2-E_1=\hbar\omega_{\rm LO}$). Following this maximum, $W_{21}^{\rm av}$ decreases as L_z increases. In dashed lines we reproduce $W_{21}^{\rm av}$ when the E_1 population is negligible. In this case there is a faster relaxation for all well widths. These curves show that the thermal average prevents the observation of a net cutoff in the vicinity of the LO-phonon energy, and they show that the occupation of final states (E_1) can produce a significant slowing down of the relaxation time.

In conclusion, we find that including an average over the thermal distribution smooths the steplike threshold expected from the emission of the LO phonons, since a substantial fraction of carriers in the second subband have enough kinetic energy to emit LO phonons. The net result is then a progressive slowing down of the relaxation process as the E_2-E_1 energy separation is reduced, in good agreement with our experimental findings. The very long relaxation time observed in the experiment of Oberli *et al.*,[14] more than 500 ps, could be due to the filling of final states that could block the carrier relaxation.

VI. SUMMARY

We have measured the intersubband relaxation time for subbands separated by more or less than the LO-phonon energy, using GaAs/$Ga_{1-x}Al_xAs$ MQW samples with different well widths. Our measurements were per-

formed by temporally resolved pump-and-probe spectroscopy. We find that, as the energy separation of MQW subbands decreases, the intersubband relaxation rate slows down, but remains in all cases investigated faster than 40 ps. Although the LO phonon is most probably the dominant energy-dissipation mechanism, no abrupt slowing down is observed when the intersubband energy separation is varied through the LO-phonon energy.

We also present a simple calculation of the intersubband relaxation rate within the momentum-conservation approximation (MCA) which allows us to interpret the basic qualitative features of our experimental results. In this approach the electronic scattering rate is averaged over the thermal distribution of carriers. Thus, the progressive slowing down of the intersubband relaxation can be understood by considering the relaxation process as a result of an average over the thermal carrier distribution. Additionally, our calculation points out the effect of the filling of final states in the intersubband relaxation time: significant occupation of the first subband can block the intersubband relaxation, and thus produce an apparent threshold.

[1]J. L. Oudar, D. Hulin, A. Antonetti, and F. Alexandre, Phys. Rev. Lett. **55**, 2074 (1985).
[2]W. H. Knox, C. Hirlimann, D. A. B. Miller, J. Shah, D. S. Chemla, and C. V. Shank, Phys. Rev. Lett. **56**, 1191 (1986).
[3]L. Schultheis, J. Kuhl, A. Honold, and C. W. Tu, Phys. Rev. Lett. **57**, 1635 (1986).
[4]J. Shah, IEEE J. Quantum Electron. **QE-22**, 1728 (1986).
[5]S. Schmitt-Rink and C. Ell, J. Lumin. **30**, 585 (1985).
[6]S. Schmitt-Rink, D. S. Chemla, and D. A. B. Miller, Phys. Rev. B **32**, 6601 (1985).
[7]R. Darling, IEEE J. Quantum Electron. **QE-24**, 1628 (1988).
[8]S. Borenstain and J. Katz, Phys. Rev. B **39**, 10 852 (1989).
[9]M. C. Tatham, J. F. Ryan, and C. T. Foxon, Surf. Sci. (to be published).
[10]B. V. Ridley, Phys. Rev. B **39**, 5282 (1989).
[11]J. K. Jain and S. Das Sarma, Phys. Rev. Lett. **62**, 2305 (1989).
[12]A. Seilmeier, H.-J. Hubner, G. Abstreiter, G. Weimann, and W. Schlapp, Phys. Rev. Lett. **59**, 1345 (1987).
[13]F. H. Julien, J.-M. Lourtioz, N. Herschkorn, D. Delacourt, J. P. Pocholle, M. Papuchon, R. Planel, and G. Le Roux, Appl. Phys. Lett. **53**, 116 (1988).
[14]D. Y. Oberli, D. R. Wake, M. V. Klein, J. Klem, T. Henderson, and H. Morkoç, Phys. Rev. Lett. **59**, 696 (1987).
[15]J. L. Oudar, I. Abram, and C. Minot, Appl. Phys. Lett. **44**, 689 (1984).
[16]R. C. Miller, A. C. Gossard, G. D. Sanders, Yia-Chung Chang, and J. N. Schulman, Phys. Rev. B **32**, 8452 (1985).
[17]J. A. Levenson, I. Abram, R. Raj, G. Dolique, J. L. Oudar, and F. Alexandre, Phys. Rev. B **38**, 13 443 (1988).
[18]E. O. Gobel, H. Jung, J. Kuhl, and K. Ploog, Phys. Rev. Lett. **51**, 1588 (1983).
[19]R. A. Hopfel, J. Shah, P. A. Wolff, and A. C. Gossard, Phys. Rev. B **37**, 6941 (1988).
[20]D. S. Chemla, D. A. B. Miller, P. W. Smith, A. C. Gossard, and W. Wiegmann, IEEE J. Quantum Electron. **QE-20**, 265 (1984).
[21]I. Abram, Phys. Rev. B **40**, 5460 (1989).
[22]J. L. Oudar, I. Abram, A. Migus, D. Hulin, and J. Etchepare, J. Lumin. **30**, 340 (1985).
[23]B. V. Ridley, J. Phys. C **15**, 5899 (1982).
[24]F. A. Riddoch and B. V. Ridley, J. Phys. C **16**, 6971 (1983).
[25]J. P. Leburton, J. Appl. Phys. **56**, 2850 (1984).
[26]S. Das Sarma and B. A. Mason, Phys. Rev. B **31**, 5536 (1985).
[27]S. M. Goodnick and P. Lugli, Superlatt. Microstruct. **5**, 561 (1989).